Contents lists available at ScienceDirect

Bioresource Technology

Employing microalga *Chlorella sorokiniana* in the biosynthesis of paramagnetic and catalytically functional manganese cluster

Marija Tanović [a], Milan Žižić [a,b], Milica Milenković [c], Zvonko Jagličić [d], Wilfred Hagen [e],
Marina Stanić [a], Dalibor Stanković [c], Snežana Kovačević [a], Dmitry Karpov [f], Primož Šket [g],
Uroš Javornik [g], Ivan Spasojević [a,*], Milena Dimitrijević [a]

[a] *University of Belgrade – Institute for Multidisciplinary Research, Kneza Višeslava 1, 11000 Belgrade, Serbia*
[b] *Elettra Sincrotrone Trieste, SS 14 km 163, 5 in Area Science Park, 34149 Basovizza, Trieste, Italy*
[c] *Faculty of Chemistry, University of Belgrade, Studentski trg 12-16, 11000 Belgrade, Serbia*
[d] *Institute of Mathematics, Physics and Mechanics & Faculty of Civil and Geodetic Engineering, University of Ljubljana, Jamova 2, 1000 Ljubljana, Slovenia*
[e] *Department of Biotechnology, Delft University of Technology, Van der Maasweg 9, 2629HZ Delft, the Netherlands*
[f] *European Synchrotron Radiation Facility, 71 Avenue des Martyrs, 38000 Grenoble, France*
[g] *Slovenian NMR Center, National Institute of Chemistry, Hajdrihova 19, 1000 Ljubljana, Slovenia*

HIGHLIGHTS

- *Chlorella sorokiniana* generates multivalent Mn-O cluster that resembles OEC.
- The cluster is paramagnetic with antiferromagnetic transition at 13 K.
- The cluster is synthesized in acidocalcosomes and can be extracted.
- The total yield of biosynthesis was 25 %
- The cluster shows catalase-like activity and susceptibility to damage by oxidants.

GRAPHICAL ABSTRACT
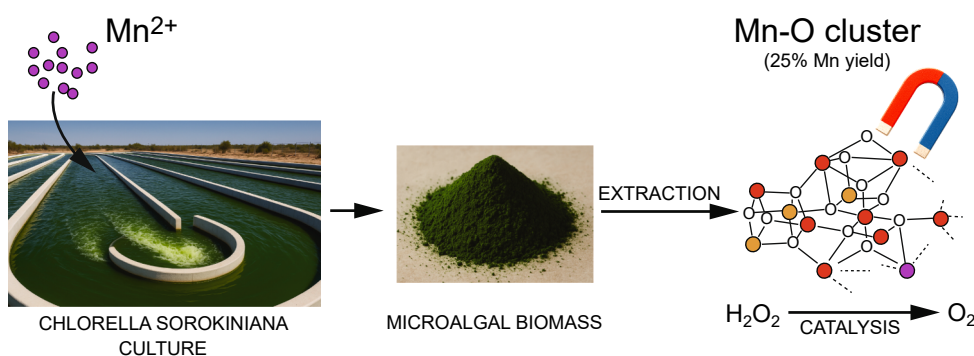
ARTICLE INFO

ABSTRACT

Finding vehicles for biosynthesis of metal clusters with advantageous magnetic and catalytic properties is an important industrial and environmental task. We have found previously that green microalga *Chlorella sorokiniana* produces a multivalent Mn-O cluster with structure that is similar to photosynthetic oxygen-evolving complex (OEC). Here we reported magnetic and redox properties and the site of accumulation of this cluster, and we proposed the mechanisms of biosynthesis and the protocol for extraction. The cluster was paramagnetic even at room temperature, with an antiferromagnetic transition at ~13 K. The separation between ground and excited state of $\Delta E \approx 15.0$ cm^{-1} matched the separation energy of OEC in S$_2$ state. Nano X-ray fluorescence microscopy and ^{31}P NMR showed that the cluster is accumulated in acidocalcosomes, a lysosome-type organelles rich in polyphosphates. The conditions in these organelles resemble the settings of chemical synthesis of OEC mimics, including mildly acidic pH and the availability of Ca^{2+} ions. Polyphosphates are likely to play a role of

* Corresponding author.
  E-mail address: ivan@imsi.bg.ac.rs (I. Spasojević).

stabilizing ligands and modulators of redox properties of Mn^{2+} in the cluster synthesis. The cluster shares redox potentials with OEC and showed catalase-like activity. However, we could not confirm OEC-like performance because the cluster was prone to degradation by oxidizing agents in the presence of organic residue in the extract. The biosynthesis showed an overall yield of ~25 % and appears to be cost-competitive with chemical synthesis. This study shows that metabolic trades of selected microalgae can be employed in the green synthesis of catalytically functional clusters.

1. Introduction

The identification of viable routes of biosynthesis of metal clusters is important for industrial catalysis, advanced photochemical and redox processes (such as artificial photosynthesis and photo-oxidation of pollutants), and the development of magnetic, photo-responsive, and sensory materials (Boncella et al., 2021). Chemical synthesis of metal clusters relies on solvothermal strategies that use toxic solvents, produce chemical waste, and commonly show long process times, high energy consumption, and low output yields. Biosynthesis using specific strains of microalgae (unicellular algae) may be a promising alternative way to make cluster synthesis more environmentally friendly and cost-effective (Hanikenne et al., 2021; Priya et al., 2022). Many microalgae inherently accumulate metals as a part of their metabolic strategies or adaptive responses (Hanikenne et al., 2021; Priya et al., 2022), and some 'use' metals to build highly-ordered structures. It is worth mentioning that a number of studies have addressed the synthesis of noble metals nanoparticles in microalgae (Dahoumane et al., 2017). However, the biosynthesis of (transition) metal clusters has been less explored. Cluster biosynthesis commonly involves the alteration of the redox state of the metal ions and development of specific magnetic and catalytic properties (Wang et al., 2017). The formation of magnetic clusters in selected microalgae and in genetically engineered strains have been reported to result in magnetotaxis (Brayner et al., 2012; de Araujo et al., 1986; Santomauro et al., 2018). This could find use in harvesting the cells from cultures, which is a critical step in microalgal industry (Li et al., 2021). Potential catalytic properties of clusters include photocatalytic, electrocatalytic, and redox activity. Microalgae-synthesized metal clusters have shown the capacity to degrade, reduce or adsorb different pollutants, such as bisphenol A (Wang et al., 2017), diclofenac (Wang et al., 2022), Cr(VI) (Subramaniyam et al., 2015), and cationic and azo dyes (Alsamhary et al., 2022; Shalaby et al., 2021), or to damage selected targets, such as pathogens (Win et al., 2021), or even malignant cells (Doman et al., 2024; Salehzadeh et al., 2019). This holds a promise for their use in environmental remediation and other fields. It is worth mentioning that a combination of magnetic and catalytic properties could be particularly beneficial from the point of simple magnetic separation and recovery of clusters after their catalytic use (Tonelli et al., 2023).

We have recently observed that the microalga *Chlorella sorokiniana* synthesizes and accumulates multivalent Mn-O cluster in the presence of an excess of manganese (Vojvodić et al., 2023). The synthesis took place in cultures in the early stationary phase of growth and required exposure to high yet sublethal concentration of Mn^{2+} (1 mM) for a prolonged period of time (72 h). The cluster has been identified by synchrotron radiation-based X-ray absorption spectroscopy. According to the predominance of Mn^{4+} and Mn^{3+} redox forms and to the distances between Mn and O and between adjacent Mn atoms, the cluster closely resembled the structure of tetramanganese cluster in the oxygen-evolving complex (OEC). Although the biosynthesis of an OEC-like cluster is intriguing, it is not completely uncommon and has been recently observed in isolated photosystem II and some macroalgae (Chernev et al., 2020; Schöler et al., 2014). Some other microalgae have been reported to accumulate Mn oxides [Chaput et al., 2019; Crawford and Heap, 1978; Wang et al., 2017). However, *C. sorokiniana* is currently the only microalga that exhibited the capacity to produce OEC-like cluster. *C. sorokiniana* is a robust, fast-growing, industrially-relevant strain with high productivity of metabolites and capacity to grow in wastewaters (Lizzul et al., 2018; Unkefer et al., 2017), which makes it a viable candidate for the commercial biosynthesis of functional clusters. The synthesis and analysis of OEC mimetics is crucial for elucidating the redox and structural determinants of biological water oxidation which is an essential component in the development of catalysts for artificial photosynthesis (Zhang et al., 2015). The chemical synthesis of the mimetics is challenging and includes multiple steps with low yields and potentially explosive intermediates (Mishra et al., 2005; Zhang et al., 2015). It appears that the biosynthesis would be a more covetable route. The biosynthesis of OEC-like clusters may help us also in understanding the evolution of the photosynthetic machinery (Chernev et al., 2020). The biotechnological potential of microalgae-produced metal clusters remained largely untapped so far. This study started with a promising candidate for the biosynthesis of catalytically-active Mn-O cluster. To understand the features of the cluster, we identified its location within *C. sorokiniana* cells, developed an extraction protocol for the purification from biomass, and examined its magnetic and catalytic/redox properties.

2. Methods and materials

2.1. Cell cultivation and cluster biosynthesis and extraction

All chemicals were of analytical or cell culture grade and were obtained from Merck (Darmstadt, Germany), if not stated differently. In all experiments deionized 18 MΩ water was used. *C. sorokiniana* strain CCAP 211/8K (Culture Collection of Algae and Protozoa, SAMS Limited, Dunbeg, UK) was used for Mn-O cluster synthesis according to the previously determined protocol (Vojvodić et al., 2023). Microalgal inocula were added to 150 mL of 3 *N*-BBM + V medium in 250 mL Erlenmeyer flasks at an initial density of 5×10^5 cells mL^{-1}. 3 *N*-BBM + V medium was prepared according to the Culture Collection of Algae and Protozoa recipe, with the initial pH of ~7.5 and the following components: $NaNO_3$ (750 mg/L), $CaCl_2 \cdot 2H_2O$ (25 mg/L), $MgSO_4 \cdot 7H_2O$ (75 mg/L), K_2HPO_4 (75 mg/L), KH_2PO_4 (175 mg/L), NaCl (25 mg/L). Na_2EDTA (4.5 mg/L), $FeCl_3 \cdot 6H_2O$ (0.582 mg/L), $MnCl_2 \cdot 4H_2O$ (0.246 mg/L), $ZnCl_2$ (0.03 mg/L), $CoCl_2 \cdot 6H_2O$ (0.012 mg/L) $Na_2MoO_4 \cdot 2H_2O$ (0.024 mg/L), and vitamins B1 (1.2 mg/L) and B12 (1.0 mg/L). The solution of mixture of inorganic salts was sterilized in autoclave. Stock solutions of vitamins were filtered through 0.2 µm filter and added to cooled sterilized medium. Cultures were grown on orbital shakers (120 rpm) in a growth cabinet at 22 °C with a continuous photon flux density of 120 µmol $m^{-2} s^{-1}$ (MST TL-D Reflex 36W840 1 SLV/25 tubes, Philips, Amsterdam, The Netherlands), for 20 days to reach stationary phase. Flasks containing samples were weighed on day 0 and the volume of the samples was corrected for evaporation with sterile water at day 15. At day 20, cultures were treated with 1 mM $MnCl_2$ for 72 h. The biomass was harvested by centrifugation at 5000g for 5 min, washed three times with water (50 mL), freeze-dried, pulverized in liquid N_2 using mortar and pestle, and stored at −20 °C. The biomass yield was similar as in the study (Vojvodić et al., 2023). These samples were used for cluster extraction, and for electron paramagnetic resonance (EPR) and magnetometry analyses.

Clusters were extracted from microalgal biomass according to the method by Villalobos and colleagues (Villalobos et al., 2003), with some modifications. The protocol is meant to release intracellular fluid through the outer rigid layer of the cell wall and to remove a significant

fraction of organic matter. Of note, the outer layer of *C. sorokiniana* cell wall is made of chitosan-like polymers (Baudelet et al., 2017), which are dissolved in chloroform (Peesan et al., 2006). In brief, freeze-dried biomass (0.5 g) was homogenized using a mortar and pestle, suspended in 10 mL of water, shaken for 10 min, and centrifuged for 5 min at 10,000*g*. Pellet was resuspended in 8 mL of 2.5 M phenol solution in Tris-Cl buffer pH = 7 (PhOH), and subjected to vortex treatment (10 min) and ultrasonic bath (2 h). The suspension was centrifuged for 15 min at 15,000*g*. The pellet was subjected to 5 cycles of vortex (10 min), sonication (20 min), and centrifugation (15 min at 15,000*g*), with the following solvents: PhOH, PhOH/CHCl$_3$ 1:1 (v/v), CHCl$_3$, methanol/CHCl$_3$/H$_2$O 12:5:3 (v/v/v) mixture, and 0.17 % NaOCl solution. The pellet was washed 4× with 10 mL of water between each of these solvents. After leaching, pellet was vortexed for 10 min and centrifuged for 5 min at 5000*g*. The remaining material was suspended in 10 mL of 0.17 % NaOCl solution and shaken for 2 h. The final pellet produced from 0.5 g of biomass was washed 4× with 10 mL of water, and suspended in 10 mL of water. Untreated biomass was processed using the same protocol to obtain control extract.

The content of Mn in the extract was determined using inductively coupled plasma–atomic emission spectroscopy on Avio 200 spectrometer (PerkinElmer, Waltham, MA, USA) with the Mn emission line at 257.610 nm. This was used to determine the yield of cluster biosynthesis, since the extraction process removed soluble/free Mn ions and Mn-containing proteins. The calculated yield represents the fraction of the total Mn used for microalgae treatment that was incorporated into the cluster(s).

2.2. Magnetic properties of the cluster

EPR spectroscopy was applied in order to obtain information about the spin states of Mn in the cluster. Perpendicular-mode EPR spectra were recorded on a Bruker EMXplus EPR spectrometer operating at X-band (9.42 GHz) at temperatures between 8 and 30 K, using the following conditions: power, 30 dB; modulation amplitude, 0.1 mT; scan time 300 s; time constant 164 ms. The signals were checked for saturation. Parallel-mode signals were obtained at 35 K, with the dual-mode cavity at 9.29 GHz, and the same conditions (except for the frequency). Doubly integrated EPR signals were corrected for temperature and plotted versus the temperature to gain additional information on the spin and to estimate ground/excited state separation. The data were fitted to a two-state system (ground state with fractional population n$_0$ and one excited state with fractional population n$_1$) according to the Boltzmann-distribution equation:

$$n_1 = n_0 e^{-\Delta E/kT} \tag{1}$$

in which ΔE is the energy separation between the two states, k = 0.695 cm^{-1}/K is the Boltzmann constant, and T (K) is the temperature, and

$$\%n_1 = 100\frac{n_1}{n_0 + n_1} = 100\frac{e^{-\Delta E/kT}}{1 + e^{-\Delta E/kT}} \tag{2}$$

DC and AC magnetic measurements were performed on the powdered dry biomass samples between 2 K and 300 K using a Quantum Design MPMS-XL-5 magnetometer. The field-cooled (FC) and zero-field-cooled (ZFC) magnetizations were carried out as a function of temperature (2–300 K). In the ZFC regime, samples were first cooled down to 2 K in the magnetic field equal to zero. Afterwards the magnetization was measuring during temperature increment up to 300 K in the presence of magnetic field of 1 kOe. For the FC measurements, the same magnetic field was applied during the cooling to 2 K. The magnetization response was then monitored during the reheating process up to 300 K. Diamagnetic contributions of the sample holders were subtracted from the collected data.

### 2.3. Subcellular localization of the cluster

Synchrotron radiation-based nano X-ray fluorescence microscopy (nano-XRF) was performed at ESRF synchrotron at ID16A beamline. The ID16A is one of very few instruments that allows elemental mapping (transition metals – Mn, Fe, Zn, as well as P, Ca, K) of individual microalgal cells (<5 μm in size) in their native states at high resolution taking advantage of 15 nm probe size. Microalgal cultures at day 20 were untreated or treated with 1 mM MnCl$_2$ for 1 h or 72 h. Cells were centrifuged at 5000 *g* for 5 min and washed three times with water. Aliquots of 5 μL suspension of microalgae were placed on silicone-nitride membrane (Silson, Southam, UK) and freeze-dried. All samples were transferred to the sample stage using Leica VCL 500 shuttle cryo system. The sample stage is positioned inside of high vacuum chamber that is necessary for both, cryo experiment and maximizing XRF signal of low-Z and low concentration elements. The overview scans of individual cells were done at 200 nm resolution. Selected cells were investigated at 25 nm spatial resolution (at least 3 cells per sample). Dwell time of the scans was set to 50 ms and the beam energy was 17.1 keV, ensuring sufficient statistics and excitation of relevant fluorescence lines. The results were processed using PyMCA software package (Solé et al., 2007).

^{31}P NMR spectroscopy was applied to elucidate the interactions of paramagnetic Mn^{2+} and Mn-O cluster with (poly)phosphates. Microalgal samples (150 mL) in the stationary phase were untreated, or treated with 1 mM MnCl$_2$ for 1 h, 24 h, and 72 h. Cells were centrifuged at 5000*g* for 5 min, washed two times with 50 mM Tris-Cl buffer pH = 7 and once with 10 mM EDTA. Fresh samples were prepared just prior to the measurements. Washed cells were suspended in 0.3 mL of TrisCl buffer containing NaHCO$_3$ (1 mM). The resulting suspensions were placed in NMR cuvettes. ^{31}P NMR spectra were acquired on a Bruker Avance NEO 600 MHz NMR spectrometer at 298 K tuned at the ^{31}P resonance frequency with 5 mm diameter tubes. External reference was set to 85 % H$_3$PO$_4$, spinning rate was set at 20 Hz, repetition rate (relaxation delay + acquisition time) was 5 s, whereas the number of scans was 240 or 1440. The spectral width was set to 17241 Hz (71.0 ppm). Transmitter frequency offset was set to −15.0 ppm. The spectra were recorded using 8192 points (TD).

2.4. Redox properties of the cluster

Cyclic voltammetry measurements were performed at room T using fresh extracts in water (pH = 6.7). The sample volume was 5 mL. The voltammograms of standards were collected on control extracts that were supplemented with MnCl$_2$, MnO$_2$, and Mn$_2$O$_3$ (0.3 g mL^{-1}, 0.13 g mL^{-1}, and 0.12 g mL^{-1}, respectively). Electrochemical measurements were performed using a potentiostat/galvanostat CHI 760b (CH Instruments, Austin, TX, USA), with conventional three-electrode cell. The electrodes were: platinum working electrode (model CHI 102, CH Instruments), Ag/AgCl (3 M KCl) reference electrode (model CHI 111, CH Instruments), and a platinum wire auxiliary electrode (model CHI 115, CH Instruments). The recording range was from −1.5 to 2 V. Scan rate was 0.1 V/s.

Room-T EPR spectra were recorded using X-band EPR spectrometer Bruker EMX Nano and the following settings: attenuation 15 dB, modulation amplitude 0.2 mT, sweep width 80 mT, scan time 180 s for the analyses of Mn(II) signal (spectrum of 1 mM of MnCl$_2$ was used as a reference). The same attenuation with modulation amplitude 0.1 mT, sweep width 10 mT, and scan time 60 s were used for free radical detection experiments using spin-trap BMPO (Cayman Chemicals, Ann Arbor, MI, USA; final concentration 8 mM). Spectral simulations for BMPO/OH adduct were performed in WINEPR SIMFONIA (Bruker Analytische Messtechnik GmbH, Karlsruhe, Germany), with the following parameters: /OH adduct: isomer I (81.6 %): aN = 1.356 mT, aH$_\beta$ = 1.23 mT, aHγ = 0.066 mT; isomer II (18.4 %): aN = 1.347 mT, aH$_\beta$ = 1.531 mT, aH$_\gamma$ = 0.062 mT (Zhao et al., 2001). Cluster extracts
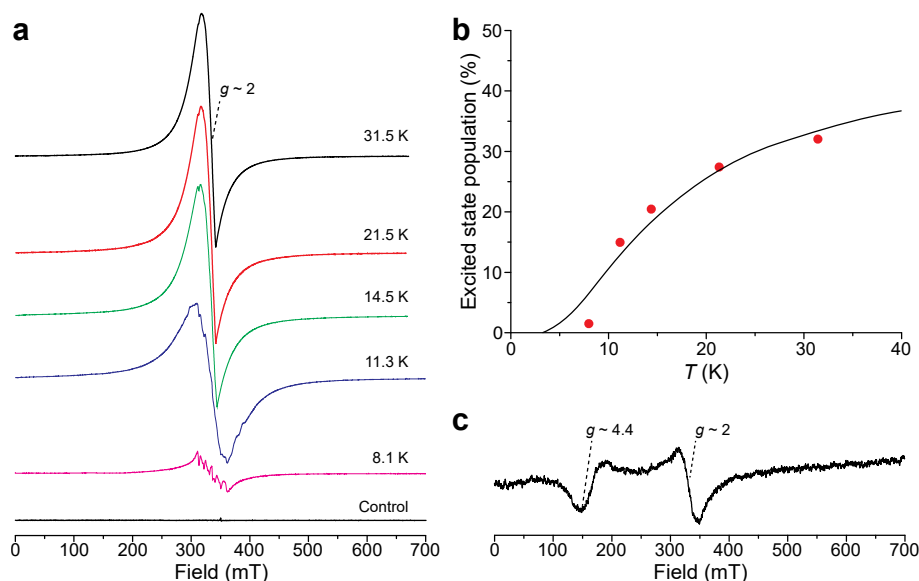
Fig. 1. Low-T EPR spectra of Mn in *C. sorokiniana* biomass. (a) Temperature plot of EPR signals of biomass with the cluster that were collected in perpendicular mode at T from 8.1 K to 31.5 K. Control biomass showed no detectable signal of Mn at 32.5 K. (b) Plot of the % of Mn ions in excited state (proportional to the doubly integrated EPR), versus the T, with a Boltzmann-population fit. Energy difference between the ground and the first excited state in Mn *d*-orbitals was $\Delta E \approx 15$ cm^{-1}. (c) Spectrum acquired in EPR parallel mode at 35 K. The strong g ~2 signal of half-integer spin cluster(s) in perpendicular mode is also visible in the parallel mode (where it is forbidden) as a weak line at the same g-value.

were treated with 10 mM cerium(IV) ammonium nitrate.

Oximetry measurements were performed using fresh extracts (pH 6.7), at room T. OEC-like activity (total reaction: $2H_2O \rightarrow O_2 + 4H^+$; electrons come from: $4Ce^{4+} \rightarrow 4Ce^{3+}$) and catalase-like activity (total reaction: $2H_2O_2 \rightarrow O_2 + 2H_2O$) were analyzed using a Clark type oxygen electrode (Hansatech Instruments Ltd., King's Lynn, UK) operating with Lab Pro interface and Logger Pro 3 software (Vernier, Beaverton, OR, USA). Air saturated water solutions ([O_2]$_{20°C}$ = 276 μM) were used for calibration of the electrode. All systems were recorded for 2–5 min before the addition of extract to establish the stability of baseline and zero rate of O_2 change at room T. Extracts (100 μL) were dissolved in 1 mL of water for these experiments. OEC-like activity was tested using strong one-electron oxidizing agent cerium(IV) ammonium nitrate (2.5 mM final concentration) according to previously described protocol (Kurz et al., 2007). It shows standard reduction potential of 1.61 V. It can oxidize Mn^{3+} to Mn^{4+} in OEC to enable water oxidation, but shows inertness in water due to saturated Ce^{4+} coordination sphere and highly hydrogen bonded secondary coordination sphere (Akbari et al., 2023; Piro et al., 2014). To reach anaerobic conditions, all solutions were purged with Ar. Catalase-like activity of cluster extract was analyzed by adding catalase substrate H_2O_2 (100 μM), and catalase enzyme (200 IU) as a reference. Catalase-like activity was also tested for MnCl$_2$, Mn$_2$O$_3$ and MnO$_2$ (50 μM final concentration) in control extracts, which were used for reference.

2.5. Statistics

Statistical analysis was performed in STATISTICA 8.0 (StatSoft Inc., Tulsa, OK, USA) using Mann–Whitney test ($p < 0.05$).

3. Results and discussion

#### 3.1. Magnetic properties of the cluster

The Mn-O cluster in *C. sorokiniana* biomass showed EPR signal at $g = 2$ (Fig. 1a). EPR line at this position is present for S$_0$ state of OEC cluster (contains Mn^{4+} and 3Mn^{3+}) (Britt et al., 2000), and for S$_2$ state (contains 3Mn^{4+} and Mn^{3+}), which usually shows an additional peak at ~4.9 due

to the presence of two redox/spin isomers (Zhang et al., 2015). However, the signal of the cluster here lacked hyperfine structure that is characteristic for the native OEC in chloroplasts (Zhang et al., 2015). This could be explained by a more heterogenous organization of the cluster compared to OEC, which results in a larger number of transitions and a broad featureless signal. The signal showed *T*-dependent changes in intensity and shape and 'disappeared' at lower T, which means the cluster is not in the ground state. Although the amplitudes of signals recorded at 31.5 K, 21.5 K, and 14.5 K were similar, this is, in itself, significant, because for a ground state one would expect the 31.5 K signal to be more than twice lower in amplitude than the 14.5 K signal. Nevertheless, an observable change in amplitude and shape took place at 11.3 K, implicating alterations in paramagnetic properties at T between 11.3 K and 14.5 K. Similar broad $g = 2$ signals with analogous *T*-dependence have been observed previously for some OEC-model clusters (Kanady et al., 2013; Van Allsburg, 2016). Such spectral changes are indicative of exchange-coupled spin systems with dominant antiferromagnetic couplings. At higher temperatures, states with larger spins are populated and the transition between spin levels of these states have larger probabilities giving rise to increased signal intensity (Kanady et al., 2013). At T = 8.1 K, a weak signal remains that is typical for mononuclear, non-specifically bound Mn^{2+}, on top of the strongly reduced main signal. This is in line with the previous findings that biomass with cluster also contains some Mn^{2+} (Vojvodić et al., 2023). We fitted the doubly integrated EPR signals corrected for T versus T to a Boltzmann distribution of states. For a ground state $S = 1/2$, this would give a straight horizontal line according to Curie's law. The data were fitted to a two-state system (ground state with fractional population n$_0$ and one excited state with fractional population n$_1$) according to the Boltzmann-distribution. The fit gives a ground state to excited state separation of $\Delta E \approx 15.0$ cm^{-1} (Fig. 1b). This ΔE value matches the separation energy between the ground and first excited-state of OEC in S$_2$ state (Kulik et al., 2007; Lohmiller et al., 2012). However, we do not know the total spin of the system here; if there are more excited states (*e. g.*, $S = 5/2$; $D < 0$), then the 15 cm^{-1} is just an approximation to the first splitting. Finally, parallel mode EPR showed a weak signal at g ~4.4, which means that cluster shows a redox state with integer spin (Fig. 1c). Pertinent to this, S$_1$ and S$_3$ states of OEC cluster have integer spins and
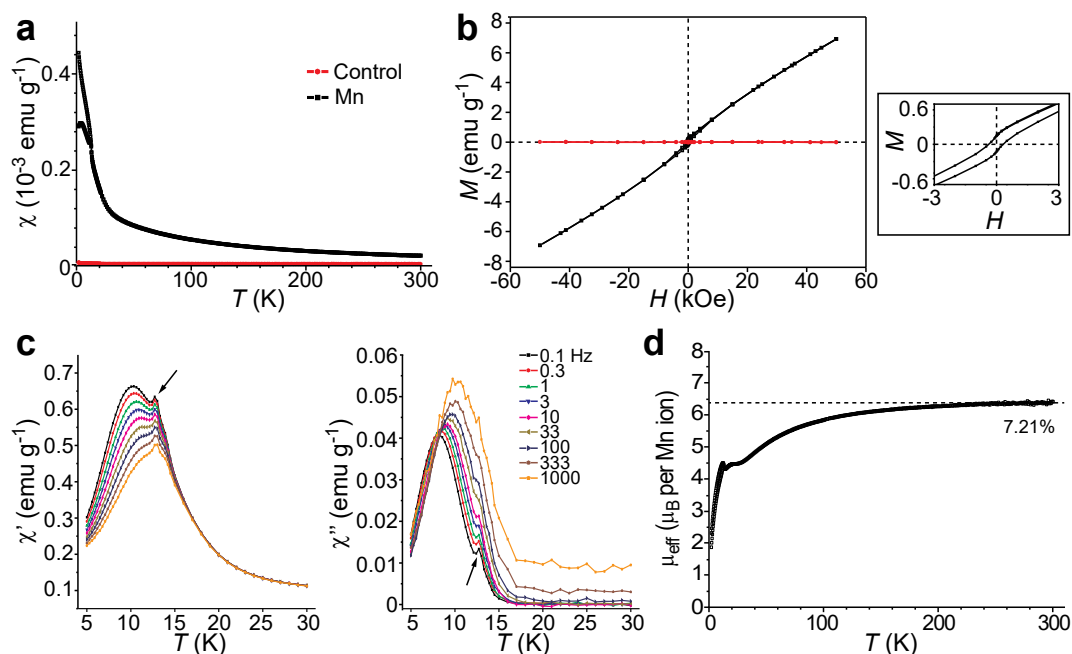
Fig. 2. Magnetometric analyses of biomass of microalgae treated Mn. Cultures were treated with 1 mM MnCl$_2$ and compared to untreated (control) cultures. (a) Zero-field-cooled (ZFC)/field-cooled susceptibility (FC) curve at 1 kOe field. (b) Hysteresis loops M(H) at 2 K. Inset show enlarged hysteresis loop for the cluster. (c) AC susceptibility data (in-phase (left) and out-phase (right)) around antiferromagnetic transition T for Mn treated sample. The peak in susceptibility at 13 K (arrow) comes from the transition. (d) The dependence of the effective magnetic moment on T (applied field 1 kOe). The content of Mn in the biomass was 72.1 mg g^{-1}. μ_B – Bohr magneton.
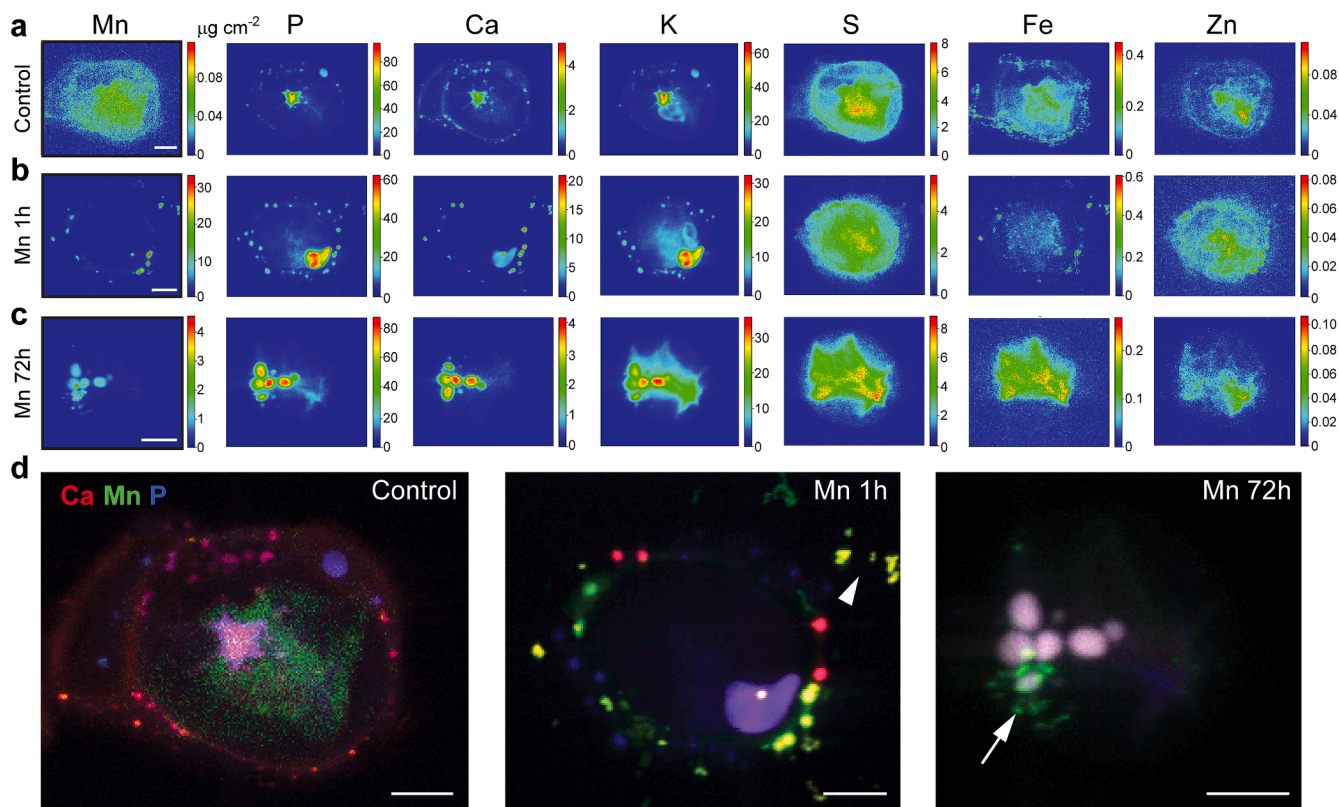
Fig. 3. Element distribution maps of *C. sorokiniana* cells generated using nano-XRF. Quantitative maps ($\mu g \, cm^{-2}$) of Mn, P, Ca, K, S, Fe, and Zn are presented for: (a) untreated microalgae; (b) microalgae treated with 1 mM MnCl$_2$ for 1 h; and (c) microalgae treated with 1 mM MnCl$_2$ for 72 h. Pseudo-color scales correspond to the concentration for each element (blue – min; red – max). (d) Overlay of three elements, where Ca contributes the red, Mn the green, P the blue color. Arrowhead – Mn deposits in the mucilage; arrow – deposits of Mn outside the acidocalcisomes. Bars in all micrographs – 1 μm.
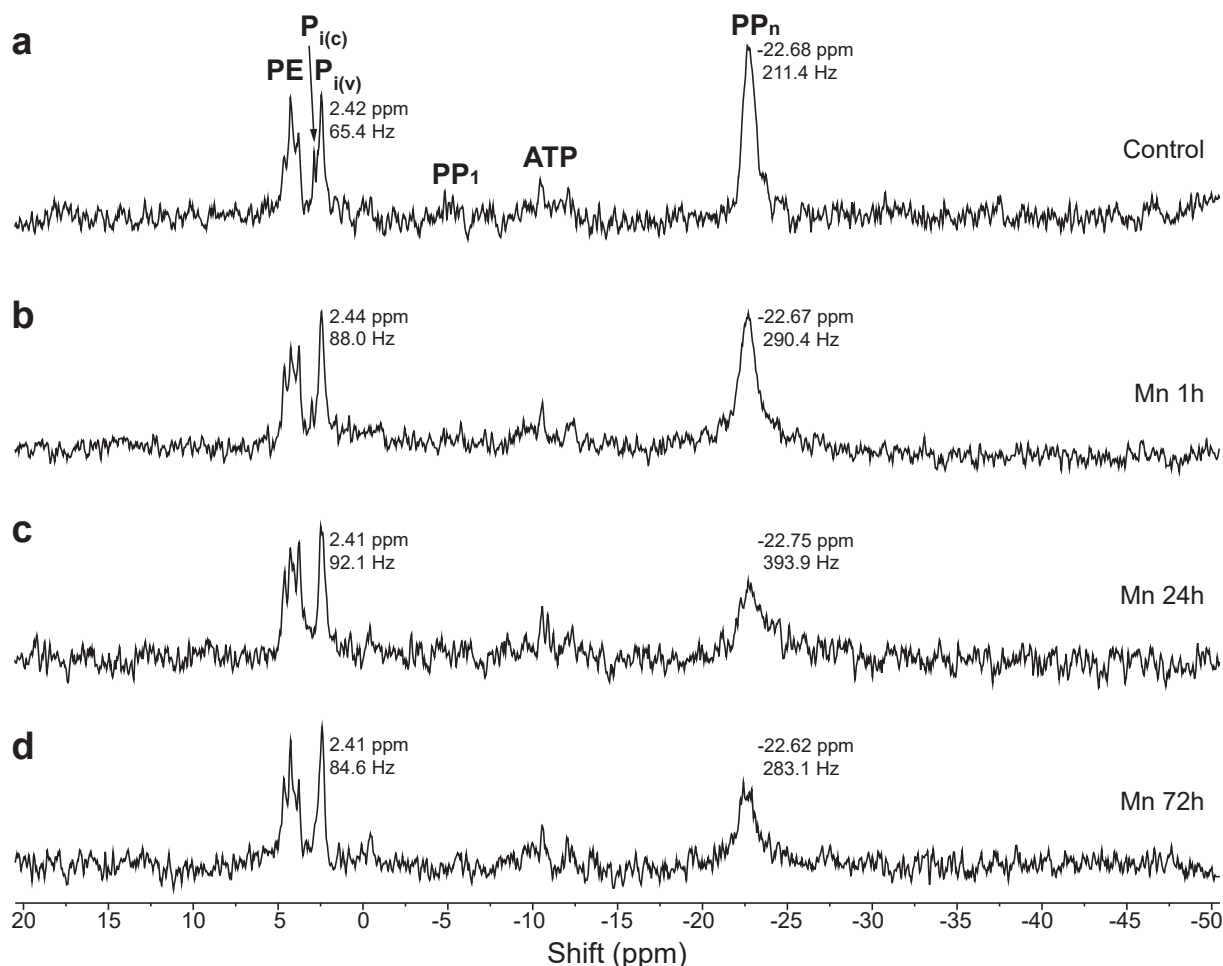
Fig. 4. ^{31}P NMR spectra of alive concentrated culture of *C. sorokiniana*. (a) Untreated cells. Cultures exposed to 1 mM MnCl$_2$ for: (b) 1 h; (c) 24 h; and (d) 72 h. NMR spectra were collected at 600 MHz and 298 K. PE – phosphoesters; Pi – orthophosphate (Pi$_{(c)}$ – in cytosol; Pi$_{(v)}$ – in vacuole); PP – polyphosphates (PP$_1$ – end phosphate groups in the polyphosphate chain; PP$_n$ – all other phosphate units in the polyphosphate). Chemical shifts (ppm) and line widths (Hz; full width at half maximum amplitude) are presented.

parallel mode EPR signals that resemble the signal here (Britt et al., 2000; Hsieh et al., 2024; Matsukawa et al., 1999).

The cluster showed paramagnetic properties at room T (Fig. 2). Biomass without cluster (control) was diamagnetic. The cluster showed antiferromagnetic transition at 13 K (Fig. 2a, c), which is in accord with temperature dependence of EPR signal of the cluster (Fig. 1a). The splitting of ZFC and FC curves at 13 K speaks in favor of the presence of a long-range coupling. Such low transition temperatures have been reported for tetramanganese and larger Mn-O clusters inserted into organic networks (Boskovic et al., 2003; Kampert et al., 2010; Kuroda-Sowa et al., 2003; Miyasaka et al., 2006). It is noteworthy that this transition temperature is much lower than for Mn oxides: 20–92 K for MnO$_2$ (a range for different crystallographic forms) (Zhou et al., 2018); 43 K for Mn$_3$O$_4$ (Narayani, et al., 2019); 49 K for Mn$_2$O$_3$ (Cong et al., 2018); 118 K for MnO (Paddison et al., 2018). This confirms that the *C. sorokiniana*-produced cluster has distinctive features compared to Mn oxides. Hysteresis measurements showed close-to-linear dependence between *M* and *H* and small hysteresis (Fig. 2b), which is probably related to canted antiferromagnetism. Alternatively, this could be related to inhomogeneity of Mn-O clusters with dominant antiferromagnetic organization and a small contribution of a ferromagnetic component. The effective magnetic moment (μ_{eff}) per Mn ion at room T was ~6.4 μ_B. This is higher than the spin-only μ_{eff} for manganese ions that make the cluster: $\mu_{eff} = 4$ μ_B for Mn^{4+} (with $S = 3/2$), $\mu_{eff} = 5$ μ_B for Mn^{3+} ($S = 2$), and $\mu_{eff} = 5.9$ μ_B for Mn^{2+} ($S = 5/2$). An explanation for

the increase in the magnetic signal at room temperature could be ferromagnetic impurities in the sample, such as accumulated iron. However, the measured $M(H)$ dependence at 300 K was linear (not shown), which rules out such an explanation. Finally, we calculated that effective magnetic moment of a single Mn-doped *C. sorokiniana* cell at room T. It was 1.7×10^{-11} emu per cell at magnetic field of 5 T and 3.2×10^{-11} emu per cell at 1 T. The calculus took into account that approximately 6.5×10^{10} cells were needed to obtain 1 g of dry biomass. Santomauro and colleagues have shown that Tb^{3+}-loaded *Chlamydomonas reinhardtii* shows an effective magnetic moment of 1.6×10^{-11} emu per cell which was the basis for magnetotaxis (Santomauro et al., 2018). However, they have claimed superparamagnetic behavior, which was not the case here.

### 3.2. Localization of the cluster biosynthesis

Nano-XRF was applied for a simultaneous mapping of Mn and other elements (P, Ca, Fe, Cl, S, Zn) within a single cell. The known distribution of P, Ca, Fe, Cl, S, and Zn was used to identify cellular compartments and to determine subcellular localization of the clusters. Element maps of untreated microalgae showed low Mn concentrations (<0.1 μg cm^{-2}) throughout the whole cell (Fig. 3a). The region with the highest Mn levels overlapped with high S and Fe concentrations, and most likely represents chloroplast (Deng et al., 2018; Leonardo et al., 2014; Schmollinger et al., 2023). Zn was located complementary to Fe, *i.e.*

outside the chloroplast, as reported previously. The region with the highest S concentrations could represent pyrenoid (Deng et al., 2018). P, Ca, and K were co-localized in acidocalcisomes, acidic organelles with dense content high in polyphosphates, Ca^{2+} ions and other cations (Goodenough et al., 2019; Lander et al., 2016; Schmollinger et al., 2021; Tsednee et al., 2019), and in the cell wall, which contains poly-phosphates that act as a sink for cations (Vojvodić et al., 2020). After 1 h of treatment, increased levels of Mn were present throughout the whole cell wall and mucilage (Fig. 3b). The latter was evident in the overlay presentation in Fig. 3d. Deposits with peak Mn concentrations mainly formed in phosphate-rich loci. The number of these loci was higher than controls. Cell wall polyphosphates appear also to sink Ca^{2+} and Fe ions from the medium. Inside the cells, P and Ca were co-localized with K in acidocalcisomes. The accumulation of P in response to the treatment with Mn has been reported previously for *C. sorokiniana* (Vojvodić et al., 2023). After 72 h, Mn was no longer present at high levels in the cell wall (Fig. 3c). Pertinent to this, the presence of phosphate-rich loci with ac-cumulations of positive ions in the cell wall was diminished. Mn was accumulated inside the cell, within acidocalcisomes that could be clearly identified as round structures with significant concentrations of P, Ca, and K. The number and size of acidocalcisomes were larger than after 1 h


(Fig. 3c). The accumulation of an excess of Mn in the acidocalcisomes has been reported for other microalgae (Tsednee et al., 2019). The overlay of maps for Ca, Mn, P (red, green, blue) and concomitant alteration of the way that the distribution of each element was presented (threshold level-based instead of concentration-based) revealed that some Mn-O clusters were accumulated in observable deposits/nano-particles that were 50–150 nm in diameter (Fig. 3d). Some of the de-posits were located outside the acidocalcisomes, probably in contractile vacuole or cytosol. Acidocalcisomes have been reported to fuse with contractile vacuoles which probably represent the final storage for the processed content of the acidocalcisomes (Goodenough et al., 2019; Lander et al., 2016).

The localization of Mn in acidocalcisomes was further confirmed by ^{31}P NMR spectroscopy (Fig. 4). Manganese ions are paramagnetic and relaxation agents that cause line broadening of spectral lines of (poly) phosphates that they bind (Ding et al., 2010; Lacerda et al., 2021). The assignment of signals was performed according to previous ^{31}P NMR studies of alive microalgal cultures (Elgavish et al., 1980; Lundberg et al., 1989). After 1 h of incubation, the signals of ortho- and poly-phosphates were broadened (Fig. 4b). According to co-localization of Mn and P that was determined by nano-XRF, this should be mainly related to interactions of Mn^{2+} with (poly)phosphates in the cell wall. The line broadening was drastically pronounced at 24 h (Fig. 4c), which is the result of Mn^{2+} influx and interactions with polyphosphates in acidocalcisomes [12]. Finally, at 72 h the broadening was partially reversed (Fig. 4d). This may be related to the formation of the clusters, which may prevent direct interactions of Mn with the polyphosphates. Alternatively, the reversibility of broadening may come as a result of the transfer of a part of the clusters from acidocalcisomes to contractile vacuole which decreases the impact of the clusters on the bulk magnetic susceptibility around polyphosphates. It is important to note that there were no changes in the linewidth for 3–5 ppm signals of phosphoesters (mainly sugar-phosphates). For orthophosphates, the line broadening may come as result of interactions with Mn or due to changes of pH in the cytosol and/or vacuole that causes the shift and overlap of pertinent signals.

Herein we amalgamated information from the presented results and previous studies to propose the mechanism of Mn-O cluster synthesis in *C. sorokiniana*. Mn^{2+} ions first accumulate in the cell wall and mucilage. Then they are transported into the cells and coordinated by poly-phosphates in acidocalcisomes. This creates conditions for the nucle-ation of clusters. The conditions in acidocalcisomes resemble the settings of chemical synthesis of OEC mimics (Mishra et al., 2005; Mukherjee et al., 2012; Shevchenko et al., 2014; Zhang et al., 2015), such as reaction medium with mildly acidic pH (acidocalcisomes show pH 5–5.5 (Goodenough et al., 2019); chemical synthesis is commonly performed at pH 5–6), availability of stabilizing ligands (phosphates in acidocalcisomes; phosphates, carboxylates, histidine in chemical syn-thesis), availability of Ca^{2+}, room temperature, and pro-oxidative con-ditions. It is noteworthy that the sites of previously reported OEC-like clusters biosynthesis also show acidic pH (Chernev et al., 2020; Schöler et al., 2014). The oxidation in the chemical synthesis is commonly performed using manganese compounds, $KMnO_4$ or tetramethylammonium-permanganat. Pertinent to this, multiple reports identified coordination complexes of Mn^{2+} with phosphates as redox reactions mediators that traverse through multiple oxidation states (Jin et al., 2014; Yang et al. 2024a; Yang et al., 2024b). With octahedral geometry and coordination of Mn^{2+} to four (or more) oxygen atoms from phosphate groups, these complexes resemble the structure of Mn^{2+} coordinated to polyphosphates in acidocalcisomes (Vojvodić et al., 2023). Some external non-selective oxidant that is available in micro-algal cells, such as O_2 (Park et al., 2015), may initiate a controlled redox process driven by Mn-polyphosphate complex that could result in the formation of an organized multivalent Mn-O cluster. In the final step, clusters appear to be released into contractile vacuole with the content of acidocalcisomes (Goodenough et al., 2019; Lander et al., 2016).
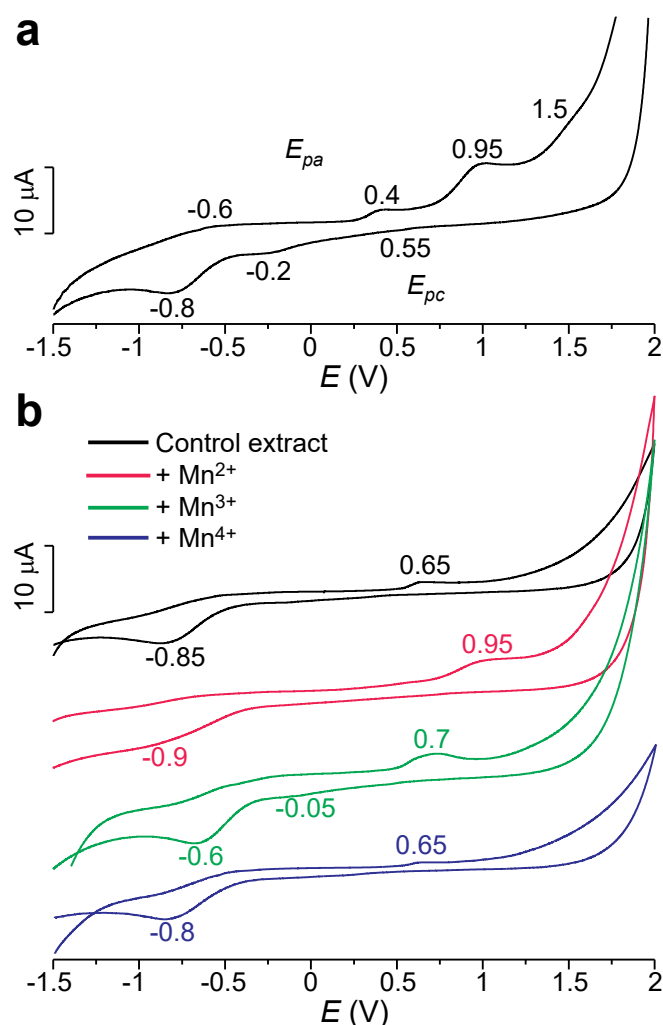
Fig. 5. Redox properties of Mn-O cluster in microalgal biomass extracts. (a) Cyclic voltammogram of extract of biomass with the cluster. (b) Cyclic vol-tammograms of the extract of control biomass in water without or with the addition of Mn. Solutions of $MnCl_2$, Mn_2O_3, and MnO_2 were used as standards for Mn^{2+}, Mn^{3+}, and Mn^{4+}. Oxidation/anodic peak current potentials (E_{pa}) and reduction/cathodic peak current potentials (E_{pc}) are labeled. pH in all systems was ~6.7.
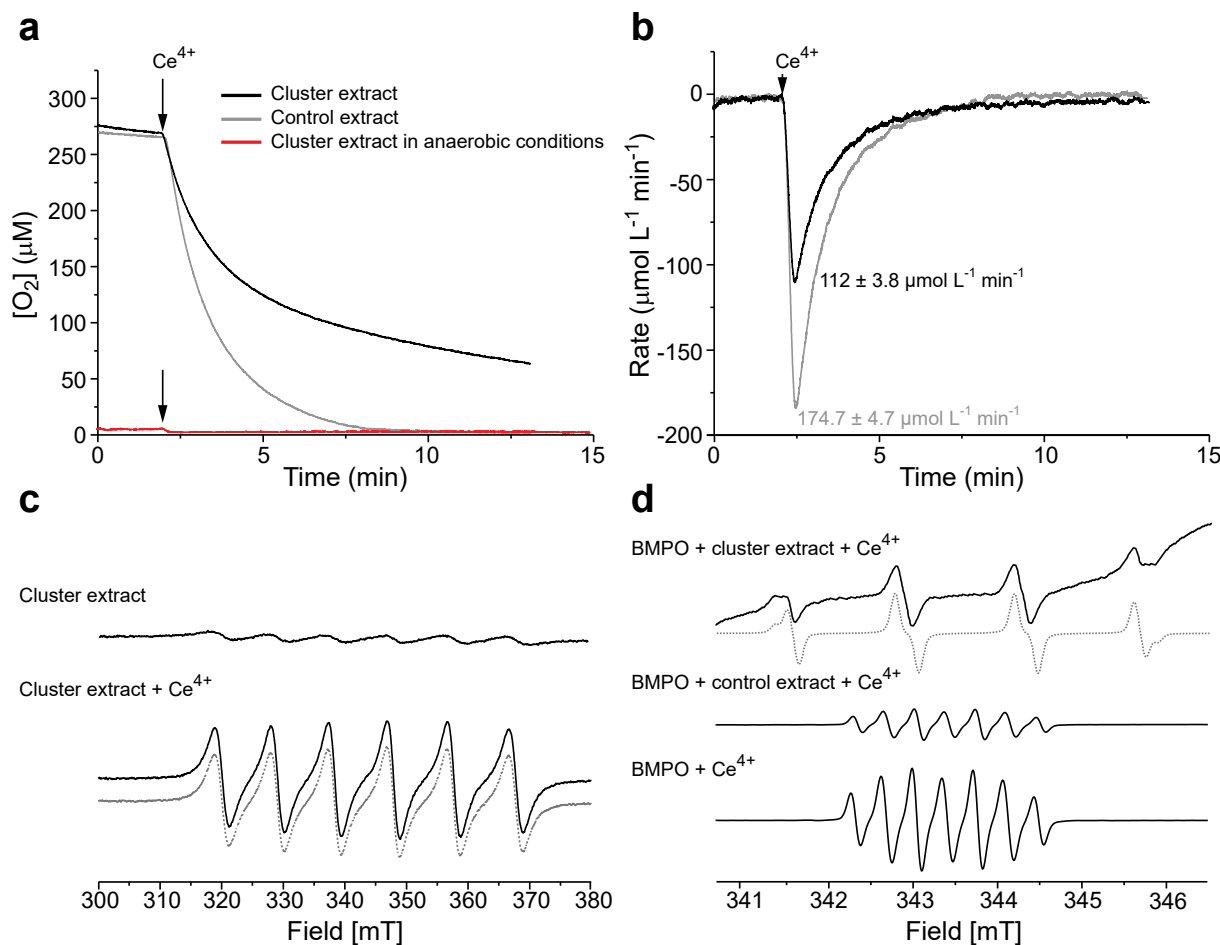
Fig. 6. The interactions of biomass extracts with oxidizing agent cerium(IV). (a) Changes in the concentration of O_2 in the water solution of cluster or control extract (100 μL per 1 mL) following the addition of 2.5 mM Ce^{4+}, were monitored to evaluate potential OEC-like activity ($2H_2O \rightarrow O_2 + 4H^+$). The activity of cluster extract was also evaluated under anaerobic conditions (samples were purged with Ar to completely remove O_2 prior to Ce^{4+} addition). (b) The rates of O_2 consumption. Mean values of maximum rates (± standard error) are presented. (c) EPR spectra of 'free' Mn^{2+} in the solution of cluster extract before and after the treatment with Ce^{4+} (10 mM). Dashed line – reference EPR spectrum of 1 mM Mn^{2+} ($MnCl_2$) in water. (d) EPR spectra of BMPO adducts after the addition of Ce^{4+} (10 mM). Dashed line – simulation of spectrum of hydroxyl radical adduct (BMPO/OH). In the absence of the cluster (in control extract or in water), Ce^{4+} causes degradation of BMPO. The obtained signal is not related to a specific adduct, but most likely comes from degradation product(s).
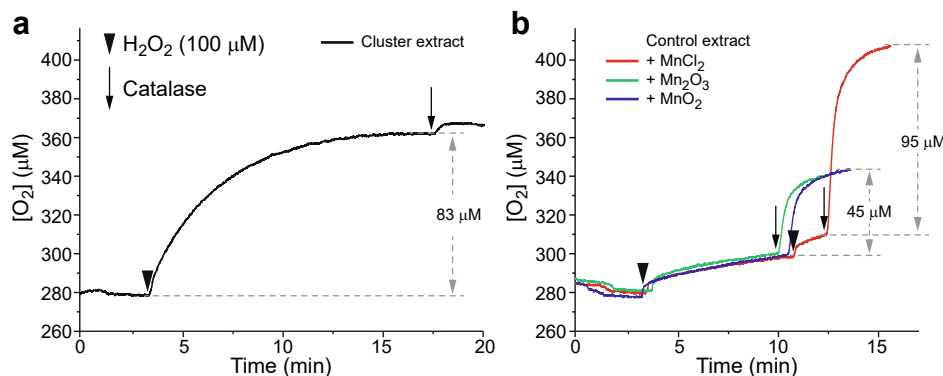
3.3. Cluster extraction

The analyses of catalytic performance benefit significantly from cluster extraction *i.e.*, removal of organic materials that may interfere with subsequent characterization of reactivity (Mandernack et al., 1995). The selection of optimal extraction approach is based on the subcellular localization of the clusters. Some microalgae accumulate Mn in the cell wall (Crawford and Heap, 1978; Wang et al., 2017), whereas in others Mn is accumulated in the intracellular compartments – vacuoles, acidocalcisomes or plastids (Smythers et al., 2023; Tsednee et al., 2019). The extraction of the cell wall fraction would require a rather different approach (Vojvodić et al., 2020), compared to the extraction from organelles (Villalobos et al., 2003). Based on the nano-XRF and ^{31}P NMR spectroscopy results, as well as this and our previous study (Vojvodić et al., 2023), we have developed protocol for production and extraction of Mn-O cluster. Briefly, *C. sorokiniana* culture was allowed to reach stationary phase, and then it is treated with 1 mM Mn^{2+} for 72 h. Biomass was thoroughly washed, collected, and freeze-dried, and clusters were extracted by the procedure that represents a modification of the method developed by Villalobos et al. (2019). More details are given in the 2.1. Cell cultivation and cluster biosynthesis and extraction. The amount of Mn that was present in the cluster extracts was compared to the initial amount of Mn that was added to microalgal culture in order to calculate the yield of biosynthesis. In average it was 25 %. This was

lower than the yield of analogous chemical syntheses. For example, Zhang et al. (2015) have reported a 50 % yield. However, this is 'compensated' by the lower cost of biosynthesis, which almost completely depends on the cost of production of dry microalgal biomass that has been estimated at <4 euro/g at industrial scale (Ruiz et al., 2016). Using current wholesale prices of all the needed chemicals we estimated that the cost of cluster production (per kg) according to the synthesis protocol of Zhang et al. (2015) is approximately 50 % higher than the cost of microalgae-based biosynthesis. More importantly, the biosynthesis does not require any use of organic solvents and does not generate hazardous waste. Of course, organic solvents were used in our extraction protocol, but taking into account magnetic properties of the cluster a large-scale extraction that relies on mechanical processing and the use of strong magnets may represent an alternative. Further optimization of the extraction process is warranted.

3.4. Redox and catalytic activity of the cluster extract

Redox properties of the cluster extract were analyzed using cyclic voltammetry (Fig. 5). It showed five distinctive peaks: three oxidation peaks (at approximately −0.6 V, 0.4 V, and 1.5 V) and two reduction peaks (at 0.55 V and −0.2 V). In addition, an oxidation peak at E_{pa} = 0.95 V that is characteristic for Mn^{2+}, and the reduction peak at E_{pc} = -0.85 V that was also observed for the control biomass extract, were

Fig. 7. Catalase-like activity of Mn-O cluster. The release of O_2 was monitored as a measure of catalase-like activity ($2H_2O_2 \rightarrow O_2 + 2H_2O$). (a) Cluster extract. (b) Different redox forms of Mn (Mn^{2+}, Mn^{3+} or Mn^{4+}) in control extract. The final concentration of $MnCl_2$, Mn_2O_3, and MnO_2 was 50 μM. The activity was tested by adding catalase substrate H_2O_2 (time points of addition are marked with arrowheads). The final concentration of H_2O_2 was 100 μM, except for the reference solution with $MnCl_2$ (H_2O_2 was added two times reaching concentration of 200 μM). Catalase enzyme (200 IU) was added after the addition of H_2O_2 to determine the amount of H_2O_2 that remained in the solution. Time points of addition of the enzyme is marked with dark arrows. The increase in O_2 concentration (in μM) is shown using dashed pale lines.

present. Peak potentials in the voltammogram of cluster extract do not reflect redox properties of Mn^{3+} and Mn^{4+} standards (Fig. 5b), which implies that they are inherent to the cluster. The obtained values resemble the oxidation and reduction peak potentials in cyclic voltammogram of OEC model compounds (of note, the voltammetry has been performed also in water using the same reference electrode type) (Zhang et al., 2015).

A potential OEC-like activity of the cluster extract was tested using oximetry and a strong oxidizing agent cerium(IV) ammonium nitrate. Unfortunately, both cluster and control extract contain significant organic residues that were oxidized by Ce^{4+} resulting in O_2 consumption (Fig. 6a). It has been shown that Ce^{4+} oxidizes biomolecules to produce carbon-centered radicals that further react with O_2 (Pottenger and Johnson, 1970). The rate of O_2 consumption was significantly higher in control extract ($p < 0.05$) (Fig. 6b), which implies that the cluster is oxidized by Ce^{4+} and that such reaction at least does not lead to O_2 consumption. The O_2 consuming effect of Ce^{4+} in the extract overshadowed potential OEC-activity of the cluster both under aerobic and anaerobic conditions. Apparently, the treatment with Ce^{4+} resulted in some degradation of the cluster since a signal of free/loosely bound Mn^{2+} became much stronger (Fig. 6c), and there was a detectable production of hydroxyl radical (Fig. 6d). In the control extract, Ce^{4+} induced a degradation of the spin-trap. This is implicated by the development of the signal that is not related to a specific spin-adduct and most likely comes from hydroxylamine products (Kálai et al., 2011).

Cluster extract showed catalase-like activity (Fig. 7a). This was not observed for control extracts supplemented with different redox forms of Mn (Fig. 7b), implying that the activity is related to the cluster, and not to the presence Mn ions *per se*. It is noteworthy that OEC in photosystem II may show catalase-like activity (Frasch and Mei, 1987), and that Mn is present in two active centers of the procaryotic non-heme manganese catalase (Whittaker, 2012). However, oxygen production did not match the stoichiometry of catalase, with more than one O_2 molecule being produced per two H_2O_2 molecules. This indicates that H_2O_2, an oxidizing agent, may induce degradation of the cluster resulting in oxygen release from its structure.

4. Conclusions

In close, we showed that microalga *C. sorokiniana* synthesize multivalent Mn-O cluster which shares magnetic and redox properties with OEC. The cluster is paramagnetic at room temperature. It is stable and can be extracted. The total yield of biosynthesis is ~25 %. The site of biosynthesis is in acidocalcisomes which provide conditions that are similar to the settings in chemical synthesis. The cluster is catalytically

functional but susceptible to degradation by the oxidizing agents that are used in activity assays. This could be related to the redox processes initiated by the agent in the organic residue in the extract. Nevertheless, the biosynthesis of OEC-like cluster opens possibilities for using this microalga in the work on the development of artificial photosynthesis, catalysts for redox processes, and magnetic materials. The synthesis and properties of this cluster may also help in understanding the place that Mn has in the evolution of oxygenic photosynthesis.

CRediT authorship contribution statement

Marija Tanović: Writing – original draft, Investigation, Formal analysis, Data curation, Conceptualization. **Milan Žižić:** Methodology, Investigation, Funding acquisition. **Milica Milenković:** Writing – original draft, Supervision, Methodology, Investigation. **Zvonko Jagličić:** Writing – original draft, Methodology, Formal analysis. **Wilfred Hagen:** Writing – original draft, Methodology, Formal analysis. **Marina Stanić:** Supervision, Investigation, Formal analysis. **Dalibor Stanković:** Methodology, Formal analysis. **Snežana Kovačević:** Investigation, Formal analysis. **Dmitry Karpov:** Methodology, Investigation, Data curation. **Primož Šket:** Methodology, Investigation. **Uroš Javornik:** Methodology, Investigation. **Ivan Spasojević:** Writing – review & editing, Writing – original draft, Visualization, Supervision, Funding acquisition, Conceptualization. **Milena Dimitrijević:** Writing – original draft, Supervision, Formal analysis.

Declaration of competing interest

The authors declare that they have no known competing financial interests or personal relationships that could have appeared to influence the work reported in this paper.

Acknowledgements

Data availability

Data will be made available on request.

References

Alsamhary, L., Al-Enazi, N.M., Alhomaidi, E., Alwakeel, S., 2022. Spirulina platensis mediated biosynthesis of Cuo Nps and photocatalytic degradation of toxic azo dye Congo red and kinetic studies. Environ. Res. 207, 112172.

Akbari, N., Nandy, S., Aleshkevych, P., Chae, K.H., Najafpour, M.M., 2023. Oxygen-evolution reaction in the presence of cerium (iv) ammonium nitrate and iron (hydr) oxide: old system, new findings. Dalton Trans. 52 (32), 11176–11186.

Baudelet, P.H., Ricochon, G., Linder, M., Muniglia, L., 2017. A new insight into cell walls of Chlorophyta. Algal Res. 25, 333–371.

Boncella, A.E., Sabo, E.T., Santore, R.M., Carter, J., Whalen, J., Hudspeth, J.D., Morrison, C.N., 2021. The expanding utility of iron-sulfur clusters: Their functional roles in biology, synthetic small molecules, maquettes and artificial proteins, biomimetic materials, and therapeutic strategies. Coord. Chem. Rev. 453, 214229.

Boskovic, C., Bircher, R., Tregenna-Piggott, P.L., Güdel, H.U., Paulsen, C., Wernsdorfer, W., Barra, A.L., Khatsko, E., Neels, A., Stoeckli-Evans, H., 2003. Ferromagnetic and antiferromagnetic intermolecular interactions in a new family of Mn4 complexes with an energy barrier to magnetization reversal. J. Am. Chem. Soc. 25 (46), 14046–14058.

Brayner, R., Coradin, T., Beaunier, P., Grenèche, J.M., Djediat, C., Yéprémian, C., Couté, A., Fiévet, F., 2012. Intracellular biosynthesis of superparamagnetic 2-lines ferri-hydrite nanoparticles using Euglena gracilis microalgae. Colloids Surf. B Biointerfaces 93, 20–23.

Britt, R.D., Peloquin, J.M., Campbell, K.A., 2000. Pulsed and parallel-polarization EPR characterization of the photosystem II oxygen-evolving complex. Annu. Rev. Biophys. Biomol. Struct. 29 (1), 463–495.

Chaput, D.L., Fowler, A.J., Seo, O., Duhn, K., Hansel, C.M., Santelli, C.M., 2019. Mn oxide formation by phototrophs: Spatial and temporal patterns, with evidence of an enzymatic superoxide-mediated pathway. Sci. Rep. 9 (1), 18244.

Chernev, P., Fischer, S., Hoffmann, J., Oliver, N., Assunção, R., Yu, B., Burnap, R.L., Zaharieva, I., Nürnberg, D.J., Haumann, M., Dau, H., 2020. Light-driven formation of manganese oxide by today's photosystem II supports evolutionarily ancient manganese-oxidizing photosynthesis. Nat. Commun. 12 (1),11, 6110.

Cong, J., Zhai, K., Chai, Y., Shang, D., Khalyavin, D.D., Johnson, R.D., Sun, Y., 2018. Spin-induced multiferroicity in the binary perovskite manganite Mn2O3. Nat. Commun. 9 (1), 2996.

Crawford, R.M., Heap, P.F., 1978. Transmission electron microscopy X-ray microanalysis of two algae of the genera Scenedesmus and Siderocelis. Protoplasma 96, 361–367.

Dahoumane, S.A., Mechouet, M., Wijesekera, K., Filipe, C.D., Sicard, C., Bazylinski, D.A., Jeffryes, C., 2017. Algae-mediated biosynthesis of inorganic nanomaterials as a promising route in nanobiotechnology–a review. Green Chem. 19 (3), 552–587.

de Araujo, F.F., Pires, M.A., Frankel, R.B., Bicudo, C.E., 1986. Magnetite and magnetotaxis in algae. Biophys. J. 50 (2), 375–378.

Deng, J., Lo, Y.H., Gallagher-Jones, M., Chen, S., Pryor Jr, A., Jin, Q., Jacobsen, C., 2018. Correlative 3D x-ray fluorescence and ptychographic tomography of frozen-hydrated green algae. Sci. Adv. 4 (11), eaau4548.

Ding, S., Xu, D., Li, B., Fan, C., Zhang, C., 2010. Improvement of 31P NMR spectral resolution by 8-hydroxyquinoline precipitation of paramagnetic Fe and Mn in environmental samples. Environ. Sci. Technol. 44 (7), 2555–2561.

Doman, K.M., Gharieb, M.M., Abd El-Monem, A.M., Morsi, H.H., 2024. Synthesis of silver and copper nanoparticle using Spirulina platensis and evaluation of their anticancer activity. Int. J. Environ. Health Res. 34 (2), 661–673.

Elgavish, A., Elgavish, G.A., Halmann, M., 1980. Intracellular phosphorus pools in intact algal cells: 31P NMR and transmission electron microscopy studies. FEBS Lett. 117 (1–2), 137–142.

Frasch, W.D., Mei, R., 1987. Hydrogen peroxide as an alternate substrate for the oxygen-evolving complex. Biochim. Biophys. Acta Bioenerg. 891 (1), 8–14.

Goodenough, U., Heiss, A.A., Roth, R., Rusch, J., Lee, J.H., 2019. Acidocalcisomes: ultrastructure, biogenesis, and distribution in microbial Eukaryotes. Protist 170 (3), 287–313.

Hanikenne, M., Esteves, S.M., Fanara, S., Rouached, H., 2021. Coordinated homeostasis of essential mineral nutrients: a focus on iron. J. Exp. Bot. 72 (6), 2136–2153.

Hsieh, W.Y., Campbell, K.A., Gregor, W., Britt, R.D., Yoder, D.W., Penner-Hahn, J.E., Pecoraro, V.L., 2024. The first spectroscopic model for the S1 state multiline signal of the OEC. Biochim. Biophys. Acta Bioenerg. 1655, 149–157.

Jin, K., Park, J., Lee, J., Yang, K.D., Pradhan, G.K., Sim, U., Jeong, D., Jang, H.L., Park, S., Kim, D., Sung, N.E., Kim, S.H., Han, S., Nam, K.T., 2014. Hydrated manganese(II) phosphate (Mn$_3$(PO$_4$)$_2$·3H$_2$O) as a water oxidation catalyst. J. Am. Chem. Soc. 136 (20), 7435–7443.

Kálai, T., Petrlova, J., Balog, M., Aung, H.H., Voss, J.C., Hideg, K., 2011. Synthesis and study of 2-amino-7-bromofluorenes modified with nitroxides and their precursors as dual anti-amyloid and antioxidant active compounds. Eur. J. Med. Chem. 46 (4), 1348–1355.

Kampert, E., Russcher, J.C., Boukhvalov, D.W., Janssen, F.F.B.J., Smits, J.M.M., de Gelder, R., de Bruin, B., Christianen, P.C.M., Rowan, A.E., Katsnelson, M.I., Maan, J. C., Zeitler, U., 2010. Antiferromagnetic interactions in a distorted cubane-type tetranuclear manganese cluster. In j. Phys: Conf. Ser. IOP Publishing. 200 (2), 022022.

Kanady, J.S., Tran, R., Stull, J.A., Lu, L., Stich, T.A., Day, M.W., Agapie, T., 2013. Role of oxido incorporation and ligand lability in expanding redox accessibility of structurally related Mn 4 clusters. Chem. Sci. 4 (10), 3986–3996.

Kulik, L.V., Epel, B., Lubitz, W., Messinger, J., 2007. Electronic structure of the Mn4O x Ca cluster in the S0 and S2 States of the oxygen-evolving complex of photosystem II based on pulse 55Mn-ENDOR and EPR spectroscopy. J. Am. Chem. Soc. 129 (44), 13421–13435.

Kuroda-Sowa, T., Nogami, T., Konaka, H., Maekawa, M., Munakata, M., Miyasaka, H., Yamashita, M., 2003. Synthesis, crystal structure and magnetic properties of novel Mn12 single-molecule magnets with thiophenecarboxylate,[Mn12O12 (O2CC4H3S) 16 (H2O) 4], and its tetraphenylphosphonium salt. Polyhedron 22 (14–17), 1795–1801.

Kurz, P., Berggren, G., Anderlund, M.F., Styring, S., 2007. Oxygen evolving reactions catalysed by synthetic manganese complexes: A systematic screening. Dalton Trans. 38, 4258–4261.

Lacerda, S., Ndiaye, D., Tóth, É., 2021. MRI relaxation agents based on transition metals. Adv. Inorg. Chem. 78, 109–142.

Lander, N., Cordeiro, C., Huang, G., Docampo, R., 2016. Polyphosphate and acidocalcisomes. Biochem. Soc. Trans. 44 (1), 1–6.

Leonardo, T., Farhi, E., Boisson, A.M., Vial, J., Cloetens, P., Bohic, S., Rivasseau, C., 2014. Determination of elemental distribution in green micro-algae using synchrotron radiation nano X-ray fluorescence (SR-nXRF) and electron microscopy techniques–subcellular localization and quantitative imaging of silver and cobalt uptake by Coccomyxa actinabiotis. Metallomics 6 (2), 316–329.

Li, X., Liu, B., Lao, Y., Wan, P., Mao, X., Chen, F., 2021. Efficient magnetic harvesting of microalgae enabled by surface-initiated formation of iron nanoparticles. Chem. Eng. J. 408, 127252.

Lizzul, A.M., Lekuona-Amundarain, A., Purton, S., Campos, L.C., 2018. Characterization of Chlorella sorokiniana, UTEX 1230. Biology 7, 25.

Lohmiller, T., Cox, N., Su, J.H., Messinger, J., Lubitz, W., 2012. The basic properties of the electronic structure of the oxygen-evolving complex of photosystem II are not perturbed by Ca2+ removal. J. Biol. Chem. 287 (29), 24721–24733.

Lundberg, P., Weich, R.G., Jensen, P., Vogel, H.J., 1989. Phosphorus-31 and nitrogen-14 NMR studies of the uptake of phosphorus and nitrogen compounds in the marine macroalgae Ulva lactuca. Plant Physiol. 89 (4), 1380–1387.

Mandernack, K.W., Fogel, M.L., Tebo, B.M., Usui, A., 1995. Oxygen isotope analyses of chemically and microbially produced manganese oxides and manganates. Geochim. Cosmochim. Acta. 59 (21), 4409–4425.

Matsukawa, T., Mino, H., Yoneda, D., Kawamori, A., 1999. Dual-mode EPR study of new signals from the S3-state of oxygen-evolving complex in photosystem II. Biochem. 38 (13), 4072–4077.

Mishra, A., Wernsdorfer, W., Abboud, K.A., Christou, G., 2005. The first high oxidation state manganese–calcium cluster: relevance to the water oxidizing complex of photosynthesis. Chem. Comm. 1, 54–56.

Miyasaka, H., Nakata, K., Lecren, L., Coulon, C., Nakazawa, Y., Fujisaki, T., Clérac, R., 2006. Two-dimensional networks based on Mn4 complex linked by dicyanamide anion: from single-molecule magnet to classical magnet behavior. J. Am. Chem. Soc. 128 (11), 3770–3783.

Mukherjee, S., Stull, J.A., Yano, J., Stamatatos, T.C., Pringouri, K., Stich, T.A., Abboud, K.A., Britt, R.D., Yachandra, V.K., Christou, G., 2012. Synthetic model of the asymmetric [Mn3CaO4] cubane core of the oxygen-evolving complex of photosystem II. Proc. Natl. Acad. Sci. USA 109 (7), 2257–2262.

Narayani, L., Angadi, V.J., Sukhdev, A., Challa, M., Matteppanavar, S., Deepthi, P.R., Pasha, M., 2019. Mechanism of high temperature induced phase transformation and magnetic properties of Mn3O4 crystallites. J. Magn. Magn. Mater. 476, 268–273.

Paddison, J.A., Gutmann, M.J., Stewart, J.R., Tucker, M.G., Dove, M.T., Keen, D.A., Goodwin, A.L., 2018. Magnetic structure of paramagnetic MnO. Phys. Rev. B 97 (1), 014429.

Park, Y.J., Matson, E.M., Nilges, M.J., Fout, A.R., 2015. Exploring Mn–O bonding in the context of an electronically flexible secondary coordination sphere: synthesis of a Mn (iii)–oxo. Chem. Commun. 51 (25), 5310–5313.

Peesan, M., Sirivat, A., Supaphol, P., Rujiravanit, R., 2006. Dilute solution properties of hexanoyl chitosan in chloroform, dichloromethane, and tetrahydrofuran. Carbohydr. Polym. 64 (2), 175–183.

Piro, N.A., Robinson, J.R., Walsh, P.J., Schelter, E.J., 2014. The electrochemical behavior of cerium (III/IV) complexes: thermodynamics, kinetics and applications in synthesis. Coord. Chem. Rev. 260, 21–36.

Pottenger, C.R., Johnson, D.C., 1970. Mechanism of cerium (IV) oxidation of glucose and cellulose. J. Polym. Sci., A-1 Polym. Chem. 8 (2), 301–318.

Priya, A.K., Jalil, A.A., Vadivel, S., Dutta, K., Rajendran, S., Fujii, M., Soto-Moscoso, M., 2022. Heavy metal remediation from wastewater using microalgae: recent advances and future trends. Chemosphere 305, 135375.

Ruiz, J., Olivieri, G., de Vree, J., Bosma, R., Willems, P., Reith, J.H., Eppink, M.H.M., Kleinegris, D.M.M., Wijffels, R.H., Barbosa, M.J., 2016. Towards industrial products from microalgae. Energy Environ. Sci. 9 (10), 3036–3043.

Salehzadeh, A., Naeemi, A.S., Khaknezhad, L., Moradi-Shoeili, Z., Shandiz, S.A.S., 2019. Fe3O4/Ag nanocomposite biosynthesised using Spirulina platensis extract and its enhanced anticancer efficiency. IET Nanobiotechnol. 13 (7), 766–770.

Santomauro, G., Singh, A.V., Park, B.W., Mohammadrahimi, M., Erkoc, P., Goering, E., Bill, J., 2018. Incorporation of terbium into a microalga leads to magnetotactic swimmers. Adv. Biosyst. 2 (12), 1800039.

Schmollinger, S., Chen, S., Merchant, S.S., 2023. Quantitative elemental imaging in eukaryotic algae. Metallomics 15 (5), mfad025.

Schmollinger, S., Chen, S., Strenkert, D., Hui, C., Ralle, M., Merchant, S.S., 2021. Single-cell visualization and quantification of trace metals in Chlamydomonas lysosome-related organelles. Proc. Natl. Acad. Sci. 118 (16), e2026811118.

Schöler, A., Zaharieva, I., Zimmermann, S., Wiechen, M., Manke, A.M., Kurz, P., Dau, H., 2014. Biogenic manganese–calcium oxides on the cell walls of the algae Chara corallina: Elemental composition, atomic structure, and water-oxidation catalysis. Eur. J. Inorg. Chem. 2014 (4), 780–790.

Shalaby, S.M., Madkour, F.F., El-Kassas, H.Y., Mohamed, A.A., Elgarahy, A.M., 2021. Green synthesis of recyclable iron oxide nanoparticles using Spirulina platensis microalgae for adsorptive removal of cationic and anionic dyes. Environ. Sci. Pollut. Res. Int. 28 (46), 65549–65572.

Shevchenko, D., Anderlund, M.F., Styring, S., Dau, H., Zaharieva, I., Thapper, A., 2014. Water oxidation by manganese oxides formed from tetranuclear precursor complexes: the influence of phosphate on structure and activity. Phys. Chem. Chem. Phys. 16 (24), 11965–11975.

Smythers, A.L., Crislip, J.R., Slone, D.R., Flinn, B.B., Chaffins, J.E., Camp, K.A., Kolling, D.R., 2023. Excess manganese increases photosynthetic activity via enhanced reducing center and antenna plasticity in Chlorella vulgaris. Sci. Rep. 13 (1), 11301.

Solé, V.A., Papillon, E., Cotte, M., Walter, P., Susini, J., 2007. A multiplatform code for the analysis of energy-dispersive X-ray fluorescence spectra. Spectrochim. Acta Part B at. Spectrosc. 62 (1), 63–68.

Subramaniyam, V., Subashchandrabose, S.R., Thavamani, P., Megharaj, M., Chen, Z., Naidu, R., 2015. Chlorococcum sp. MM11 – a novel phyco-nanofactory for the synthesis of iron nanoparticles. J. Appl. Phycol. 27, 1861–1869.

Tonelli, F.M.P., Silva, C.S., Delgado, V.M.S., Tonelli, F.C.P., 2023. Algae-based green AgNPs, AuNPs, and FeNPs as potential nanoremediators. Green Process. Synth. 12 (1), 20230008.

Tsednee, M., Castruita, M., Salomé, P.A., Sharma, A., Lewis, B.E., Schmollinger, S.R., Merchant, S.S., 2019. Manganese co-localizes with calcium and phosphorus in Chlamydomonas acidocalcisomes and is mobilized in manganese-deficient conditions. J. Biol. Chem. 294 (46), 17626–17641.

Unkefer, C.J., Sayre, R.T., Magnuson, J.K., Anderson, D.B., Baxter, I., Blaby, I.K., Brown, J.K., Carleton, M., Cattolico, R.A., Dale, T., Devarenne, T.P., Downes, C.M., Dutcher, S.K., Fox, D.T., Goodenough, U., Jaworski, J., Holladay, J.E., Kramer, D.M., Koppisch, A.T., Lipton, M.S., Marrone, B.L., McCormick, M., Molnár, I., Mott, J.B., Ogden, K.L., Panisko, E.A., Pellegrini, M., Polle, J., Richardson, J.W., Sabarsky, M., Starkenburg, S.R., Stormo, G.D., Teshima, M., Twary, S.N., Unkefer, P.J., Yuan, J.S., Olivares, J.A., 2017. Review of the algal biology program within the National Alliance for Advanced Biofuels and Bioproducts. Algal Res. 22, 187–215.

Van Allsburg, K.M., 2016. Molecular and materials investigations of Mn4O4 and Co4O4 cubanes in pursuit of artificial photosynthesis. University of California, Berkeley.

Villalobos, M., Toner, B., Bargar, J., Sposito, G., 2003. Characterization of the manganese oxide produced by Pseudomonas putida strain MnB1. Geochim. Cosmochim. Acta 67 (14), 2649–2662.

Vojvodić, S., Dimitrijević, M., Žižić, M., Dučić, T., Aquilanti, G., Stanić, M., Zechmann, B., Danilović Luković, J., Stanković, D., Opačić, M., Morina, A., Pittman, J.K., Spasojević, I., 2023. A three-step process of manganese acquisition and storage in the microalga Chlorella sorokiniana. J. Exp. Bot. 74 (3), 1107–1122.

Vojvodić, S., Luković, J.D., Zechmann, B., Jevtović, M., Bogdanović Pristov, J., Stanić, M., Lizzul, A.M., Pittman, J.K., Spasojević, I., 2020. The effects of ionizing radiation on the structure and antioxidative and metal-binding capacity of the cell wall of microalga Chlorella sorokiniana. Chemosphere 260, 127553.

Wang, Q., Liao, C., Zhao, J., Zeng, G., Liu, W., Gao, P., Sun, D., Du, J., 2022. Combined process of biogenic manganese oxide and manganese-oxidizing microalgae for improved diclofenac removal performance: Two different kinds of synergistic effects. Toxics 10 (5), 230.

Wang, R., Wang, S., Tai, Y., Tao, R., Dai, Y., Guo, J., Duan, S., 2017. Biogenic manganese oxides generated by green algae Desmodesmus sp. WR1 to improve bisphenol A removal. J. Hazard. Mater. 339, 310–319.

Whittaker, J.W., 2012. Non-heme manganese catalase–the 'other' catalase. Arch. Biochem. Biophys. 525 (2), 111–120.

Win, T.T., Khan, S., Bo, B., Zada, S., Fu, P., 2021. Green synthesis and characterization of Fe3O4 nanoparticles using Chlorella-K01 extract for potential enhancement of plant growth stimulating and antifungal activity. Sci. Rep. 11 (1), 21996.

Yang, S., Jiang, P., Yue, K., Guo, K., Yang, L., Han, J., Peng, X., Zhang, X., Zheng, H., Yang, T., Cao, R., Yan, Y., Zhang, W., 2024a. Manganese pyrophosphate with multiple coordinated water molecules for electrocatalytic water oxidation. Chin. J. Catal. 62, 166–177.

Yang, S., Yue, K., Liu, X., Li, S., Zheng, H., Yan, Y., Cao, R., Zhang, W., 2024b. Electrocatalytic water oxidation with manganese phosphates. Nat. Comm. 15 (1), 1410.

Zhang, C., Chen, C., Dong, H., Shen, J.R., Dau, H., Zhao, J., 2015. A synthetic Mn4Ca-cluster mimicking the oxygen-evolving center of photosynthesis. Science 348 (6235), 690–693.

Zhao, H., Joseph, J., Zhang, H., Karoui, H., Kalyanaraman, B., 2001. Synthesis and biochemical applications of a solid cyclic nitrone spin trap: a relatively superior trap for detecting superoxide anions and glutathiyl radicals. Free Radic. Biol. Med. 31 (5), 599–606.

Zhou, C., Wang, J., Liu, X., Chen, F., Di, Y., Gao, S., Shi, Q., 2018. Magnetic and thermodynamic properties of α, β, γ and δ-MnO 2. New J. Chem. 42 (11), 8400–8407.